An atomistic-based continuum theory for carbon nanotubes: analysis of fracture nucleation

P. Zhang[a], H. Jiang[a], Y. Huang[a,*], P.H. Geubelle[b], K.C. Hwang[c]

[a] *Department of Mechanical and Industrial Engineering, University of Illinois, 1206 W. Green Street, Urbana, IL 61801, USA*
[b] *Department of Aeronautical and Astronautical Engineering, University of Illinois, Urbana, IL 61801, USA*
[c] *Department of Engineering Mechanics, Tsinghua University, Beijing 100084, China*

Abstract

Carbon nanotubes (CNTs) display unique properties and have many potential applications. Prior theoretical studies on CNTs are based on atomistic models such as empirical potential molecular dynamics (MD), tight-binding methods, or first-principles calculations. Here we develop an atomistic-based continuum theory for CNTs. The interatomic potential is directly incorporated into the continuum analysis through constitutive models. Such an approach involves no additional parameter fitting beyond those introduced in the interatomic potential. The atomistic-based continuum theory is then applied to study fracture nucleation in CNTs by modelling it as a bifurcation problem. The results agree well with the MD simulations.
© 2003 Elsevier Ltd. All rights reserved.

Keywords: Carbon nanotube; Continuum analysis; Interatomic potential

1. Introduction

There has been extensive research on carbon nanotubes (CNTs) since their first discovery (Iijima, 1991; Ebbesen and Ajayan, 1992) and the establishment of effective synthesis techniques (Thess et al., 1996). A single-wall CNT is a cylinder of graphene with a single layer of carbon atoms, and its diameter is on the order of 1 nm. There are also multi-wall CNTs that are cylinders of graphene with multiple layers of carbon

---

* Corresponding author. Tel.: +1-217-265-5072; fax: +1-217-244-6534.
E-mail address: huang@uiuc.edu (Y. Huang).
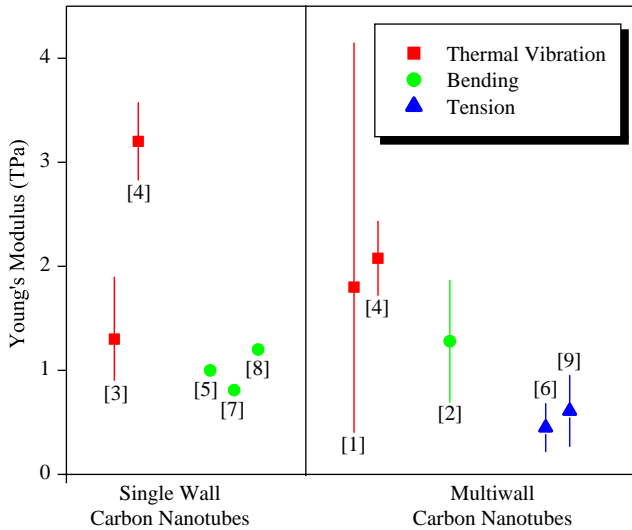
Fig. 1. Young's modulus of single and multi-wall CNTs measured by various experimental techniques: thermal vibration, bending, and tension. [1]: Treacy et al. (1996); [2]: Wong et al. (1997); [3]: Krishnan et al. (1998); [4]: Lourie and Wagner (1998); [5]: Muster et al. (1998); [6]: Pan et al. (1999); [7]: Salvetat et al. (1999); [8]: Tombler et al. (2000); [9]: Yu et al. (2000).

atoms along the tube thickness, and their diameters are much larger (e.g., 50 nm). The lengths of CNTs range from a few nanometers to 100 μm or even higher (Fan et al., 1999).

CNTs display superior mechanical properties (Srivastava et al., 2001; Yakobson and Avouris, 2001; Qian et al., 2002). Experimental studies have shown that CNTs have high Young's modulus on the order of 1 TPa, though the experimental data have very large scatterings as shown in Fig. 1. Extensive atomistic studies also show the Young's modulus of CNTs on the same order of magnitude (1 TPa), though there are also some scatterings of molecular dynamics (MD) simulations based on the empirical interatomic potential, tight-binding potential, and first-principle methods, as shown in Fig. 2. Atomistic studies also show that CNTs have yield strain more than 4% (Yakobson et al., 1996), and fracture strain ranging from 30% to 50% (Yakobson et al., 1997) based on Brenner's (1990) interatomic potential and between 10% and 16% (Belytschko et al., 2002) based on the modified Morse potential in which a bond-angle-bending term is added.

The purpose of the present study is to establish a continuum theory of CNTs based on the interatomic potential for carbon (Brenner, 1990), and to apply this atomistic-based continuum theory to study fracture nucleation in CNTs. There has been significant progress in recent years to develop continuum theories based on atomistic models for three dimensional solids (e.g., Tadmor et al. 1996a, b, 1999; Miller et al., 1998a, b; Shenoy et al., 1998, 1999) and two-dimensional planar lattice (Gao et al., 2001).
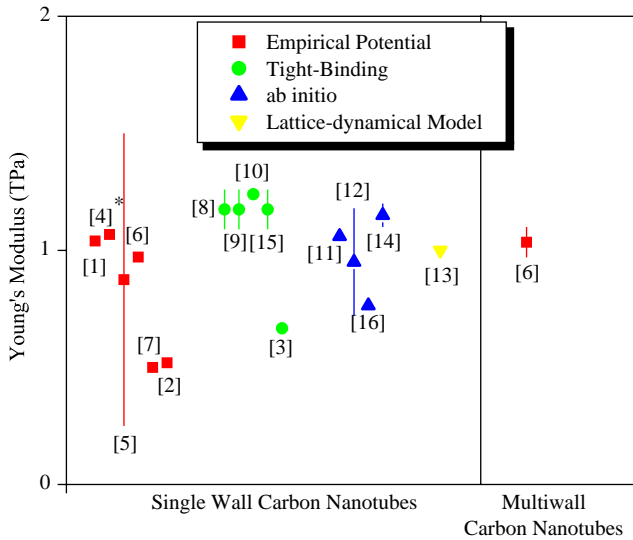
Fig. 2. Young's modulus of single and multi-wall CNTs obtained from atomic studies based on the empirical interatomic potential, tight-binding method, and ab initio calculations. [1]: Robertson et al. (1992); [2]: Overney et al. (1993); [3]: Molina et al. (1996); [4]*: Yakobson et al. (1996), the Young's modulus is obtained from the tensile stiffness using a standard CNT wall thickness 0.34 nm; [5]: Cornwell and Wille (1997); [6]: Lu (1997); [7]: Halicioglu (1998); [8]: Hernández et al. (1998); [9]: Hernández et al. (1999); [10]: Goze et al. (1999); [11]: Sánchez-Portal et al. (1999); [12]: Lier et al. (2000); [13]: Popov et al. (2000); [14]: Prylutskyy et al. (2000); [15]: Vaccarini et al. (2000); [16]: Zhou et al. (2001).

However, it is uncertain whether continuum analysis is even applicable for single wall CNTs that have only one layer of atoms. Arroyo and Belytschko (2002) used a modified Cauchy–Born rule (Weiner, 1983; Tadmor et al., 1999) to incorporate the interatomic potential into a continuum framework, and accounted for the effect of CNT curvature via an exponential map. They studied CNTs under various loadings, including torsion and bending. Zhang et al. (2002b) adopted a similar approach to study the elastic modulus and tensile stiffness of CNTs, and found good agreements with MD simulations. Though these limited continuum studies have already demonstrated some success to model CNTs it is unknown whether continuum methods can be applied to CNTs under extreme conditions such as fracture.

The purpose of this paper is to study fracture nucleation in CNTs via an atomistic-based continuum theory. The interatomic potential for carbon (Brenner, 1990), summarized in Section 2, is incorporated into a continuum constitutive model in Section 3 via the modified Cauchy–Born rule. Fracture nucleation in CNTs is modeled in Section 4 as the bifurcation in the continuum analysis. It is shown that the critical strain predicted by the atomistic-based continuum theory agrees well with MD simulations. The effect of the cutoff function on fracture nucleation in CNTs is discussed in Section 5.

2. An interatomic potential for carbon

Brenner (1990) established an interatomic potential for carbon from Tersoff (1988) formalism as

$$V(r_{ij}) = V_{\mathrm{R}}(r_{ij}) - B_{ij}V_{\mathrm{A}}(r_{ij}) \tag{1}$$

for atoms i and j, where r_{ij} is the distance between atoms i and j, V_{R} and V_{A} are the repulsive and attractive pair terms (i.e., depending only on r_{ij}) and are given by

$$V_{\mathrm{R}}(r) = \frac{D^{(e)}}{S-1}\,\mathrm{e}^{-\sqrt{2S}\beta(r-R^{(e)})} f_{\mathrm{c}}(r), \tag{2}$$

$$V_{\mathrm{A}}(r) = \frac{D^{(e)}S}{S-1}\,\mathrm{e}^{-\sqrt{(2/S)}\beta(r-R^{(e)})} f_{\mathrm{c}}(r); \tag{3}$$

the parameters $D^{(e)}$, S, β, and $R^{(e)}$ are determined from the known physical properties of carbon, graphite and diamond, and are given at the end of this section; the function f_{c} is merely a smooth cutoff function to limit the range of the potential, and is given by

$$f_{\mathrm{c}}(r) = \begin{cases} 1, & r < R^{(1)}, \\ \dfrac{1}{2}\left\{1 + \cos\left[\dfrac{\pi(r - R^{(1)})}{R^{(2)} - R^{(1)}}\right]\right\}, & R^{(1)} < r < R^{(2)}, \\ 0, & r > R^{(2)}, \end{cases} \tag{4}$$

which is continuous and has a cutoff of $R^{(2)} = 0.2$ nm and $R^{(1)} = 0.17$ nm to include only the first-neighbor shell for carbon.

The parameter B_{ij} in Eq. (1) represents a multi-body coupling between the bond from atom i to atom j and the local environment of atom i, and is given by

$$B_{ij} = \left[1 + \sum_{k(\neq i,j)} G(\theta_{ijk}) f_{\mathrm{c}}(r_{ik})\right]^{-\delta}, \tag{5}$$

where k represents atoms other than i and j, r_{ik} is the distance between atoms i and k, f_{c} is the cutoff function in Eq. (4), θ_{ijk} is the angle between bonds i–j and i–k, and the function G is given by

$$G(\theta) = a_0\left[1 + \frac{c_0^2}{d_0^2} - \frac{c_0^2}{d_0^2 + (1 + \cos\theta)^2}\right]. \tag{6}$$

For atoms i and j having different local environment, Brenner (1990) suggested to replace the coefficient B_{ij} in Eq. (5) by

$$\bar{B}_{ij} = (B_{ij} + B_{ji})/2. \tag{7}$$

The parameters $D^{(e)}$, S, β and $R^{(e)}$ in Eqs. (2) and (3), δ in Eq. (5), and a_0, c_0 and d_0 in Eq. (6) have been determined by Brenner (1990) to fit the binding energy and lattice constants of graphite, diamond, simple cubic and face-centered-cubic

structures for pure carbon, as well as the vacancy formation energy for diamond and graphite as

$$D^{(e)} = 6.000 \text{ eV}, \quad S = 1.22, \quad \beta = 21 \text{ nm}^{-1}, \quad R^{(e)} = 0.1390 \text{ nm},$$

$$\delta = 0.50000, \quad (8)$$

$$a_0 = 0.00020813, \quad c_0 = 330, \quad d_0 = 3.5.$$

Here $R^{(e)} = 0.1390$ nm represents the equilibrium bond length for a pair of carbon atoms (i.e., no other atoms such that $B_{ij} = 1$) and it is determined from $(\partial/\partial r_{ij})(V_R - V_A)|_{r_{ij}=R^{(e)}} = 0$. For a single-wall CNT having a hexagonal lattice structure within the tube surface, the equilibrium bond length l_0 is determined from

$$\frac{\partial V}{\partial r_{ij}} = 0, \quad (9)$$

where V is the interatomic potential accounting for the multi-body coupling effect (i.e., $B_{ij} \neq 1$) in Eq. (1). The equilibrium bond length determined from Eq. (9) is $l_0 = 0.145$ nm, which agrees well with the well-known bond length of graphite (0.144 nm).

3. An atomistic-based continuum theory for CNTs

Single-wall CNTs can be grouped to the following three categories according to their chiralities (the orientation of tube axis with respect to the hexagonal lattice structure):

(1) armchair nanotubes where the tube axis is normal to a lattice direction, i.e., the angle between an atomic bond and the tube axis $\phi_0 = 30°$ (Fig. 3a);
(2) zigzag nanotubes where the tube axis is parallel to a lattice direction, i.e., $\phi_0 = 0°$ (Fig. 3a);
(3) chiral nanotubes where the tube axis is neither parallel nor normal to the lattice directions, i.e., $0° < \phi_0 < 30°$ (Fig. 3a).

3.1. Modified Cauchy–Born rule

Unlike MD simulations that keep track of the motion of every atom, the atomistic-based continuum theory developed in this section represents the collective behavior of atoms via the constitutive model. The Cauchy–Born rule (Born and Huang, 1954; Milstein, 1980) equated the strain energy at the continuum level to the energy stored in atomic bonds. Moreover, atoms are subject to homogeneous deformation such that they move according to a single mapping from the undeformed to deformed configurations. Such a mapping is characterized by the continuum deformation gradient $\boldsymbol{F}$ of a material point, where the material point represents many atoms that undergo locally uniform deformation. For simple Bravais lattice that has the centrosymmetric atomic structure, the Cauchy–Born rule ensures the equilibrium of atoms. However, it does
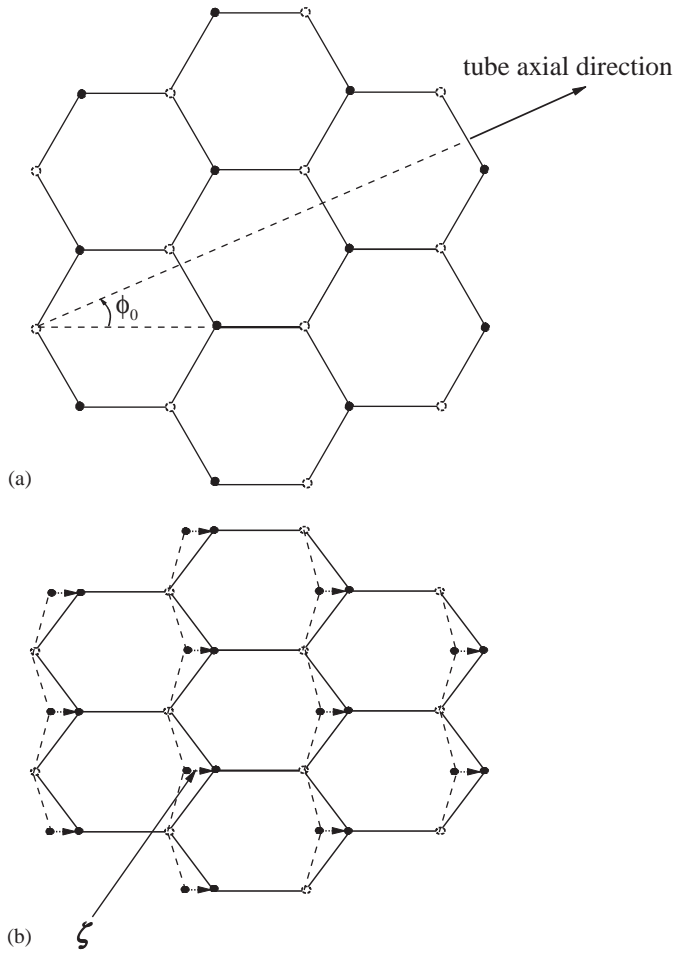
Fig. 3. (a) The decomposition of a hexagonal lattice to two triangular sub-lattices. The angle ϕ_0 shows the orientation of tube axial direction of CNT. (b) A shift vector ζ between two sub-lattices is introduced to ensure the equilibrium of atoms. The solid and dashed lines denote the lattice structures with and without the shift vector ζ, respectively.

not for the hexagonal lattice structure (Fig. 3a) which is a Bravais multi-lattice and does not possess centrosymmetry, as pointed out by Zhang et al. (2002b) for CNTs, and Tadmor et al. (1999) and Arroyo and Belytschko (2002) for general Bravais multi-lattice.

As shown in Fig. 3a, we adopt the approach of Weiner (1983), Tadmor et al. (1999), and Arroyo and Belytschko (2002) to decompose the hexagonal lattice structure to two triangular sub-lattices marked by open and solid circles. Each sub-lattice is a simple Bravais lattice that has the centrosymmetry and therefore follows the Cauchy–Born rule. However, the two sub-lattices undergo a shift vector ζ (Weiner, 1983;

Tadmor et al., 1999), as shown in Fig. 3b, which represents the relaxation of atom positions in the hexagonal lattice structure in order to minimize the energy and reach the equilibrium.

Let $\boldsymbol{r}_{ij}^{(0)} = r_{ij}^{(0)} \boldsymbol{n}_{ij}^{(0)}$ denote the vector between two atoms i and j on the CNT prior to deformation, $r_{ij}^{(0)}$ and $\boldsymbol{n}_{ij}^{(0)}$ be the bond length and unit vector, respectively. For atoms i and j within the same sub-lattice, the vector $\boldsymbol{r}_{ij}$ after the deformation becomes

$$\boldsymbol{r}_{ij} = \boldsymbol{F} \cdot \boldsymbol{r}_{ij}^{(0)}, \tag{10}$$

and its length is

$$r_{ij}(\boldsymbol{E}) = \sqrt{\boldsymbol{r}_{ij} \cdot \boldsymbol{r}_{ij}} = r_{ij}^{(0)} \sqrt{1 + 2\boldsymbol{n}_{ij}^{(0)} \cdot \boldsymbol{E} \cdot \boldsymbol{n}_{ij}^{(0)}}, \tag{11}$$

where $\boldsymbol{E} = \frac{1}{2}(\boldsymbol{F}^{\mathrm{T}} \cdot \boldsymbol{F} - \boldsymbol{I})$ is the Lagrangian strain. For atoms i and j from two different sub-lattices, the vector $\boldsymbol{r}_{ij}$ after the deformation also depends on the shift vector $\boldsymbol{\zeta}$ between the two sub-lattices, and is given by

$$\boldsymbol{r}_{ij} = \boldsymbol{F} \cdot \boldsymbol{r}_{ij}^{(0)} + \boldsymbol{\zeta} = r_{ij}^{(0)} \boldsymbol{F} \cdot (\boldsymbol{n}_{ij}^{(0)} + \boldsymbol{\xi}), \tag{12}$$

where $\boldsymbol{\xi} = (1/r_{ij}^{(0)})\boldsymbol{F}^{-1} \cdot \boldsymbol{\zeta}$ is an internal degree of freedom which is equivalent to the shift vector $\boldsymbol{\zeta}$. The bond length becomes

$$r_{ij}(\boldsymbol{E}, \boldsymbol{\xi}) = \sqrt{\boldsymbol{r}_{ij} \cdot \boldsymbol{r}_{ij}} = r_{ij}^{(0)} \sqrt{(\boldsymbol{n}_{ij}^{(0)} + \boldsymbol{\xi}) \cdot (\boldsymbol{I} + 2\boldsymbol{E}) \cdot (\boldsymbol{n}_{ij}^{(0)} + \boldsymbol{\xi})}, \tag{13}$$

which depends on both $\boldsymbol{E}$ and $\boldsymbol{\xi}$.

3.2. Continuum strain energy density

Fig. 4 shows the schematic diagram illustrating the present approach to obtain the strain energy density from the interatomic potential. The energy stored in the bond between carbon atoms i and j is given by Brenner's (1990) multi-body interatomic potential in Eq. (1),

$$V(\boldsymbol{E}, \boldsymbol{\xi}) = V(r_{ij}; r_{ik}, \theta_{ijk}, k \neq i, j), \tag{14}$$

where k denotes atoms other than i and j, the bond lengths r_{ij} and r_{ik} are given in terms of the Lagrangian strain $\boldsymbol{E}$ and internal degree of freedom $\boldsymbol{\xi}$ via (11) or (13), and the angle θ_{ijk} between deformed bonds i–j and i–k is determined from r_{ij}, r_{ik} and r_{jk}.

Based on the Cauchy–Born rule, the strain energy density W on the continuum level is the energy (stored in atomic bonds) per atom. Each atom i has three neighboring atoms in a hexagonal lattice structure such that the strain energy density W becomes

$$W(\boldsymbol{E}, \boldsymbol{\xi}) = \frac{1}{2} \frac{\sum_{1 \leqslant j \leqslant 3} V(r_{ij}; r_{ik}, \theta_{ijk}, k \neq i, j)}{\Omega_{\varepsilon}} \tag{15}$$

if only the nearest-neighbor interaction is accounted for, where V is Brenner's (1990) interatomic potential for carbon given in (1); the factor $\frac{1}{2}$ represents the equal split of
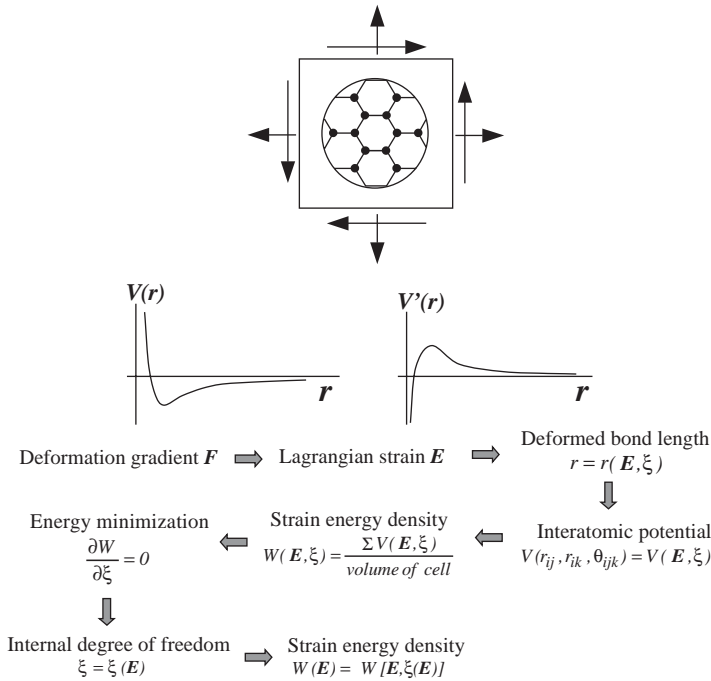
Fig. 4. A schematic diagram to link the continuum analysis to the interatomic potential for CNTs possessing no centrosymmetric atomic structure.

bond energy between two atoms in each pair;

$$\Omega_\varepsilon = \frac{3\sqrt{3}}{4}\, l_0^2 t_0 \tag{16}$$

is the average volume per atom, l_0 is the unstretched bond length for the hexagonal lattice structure in Fig. 3b and its value is reported at the end of Section 2; t_0 is the "tube thickness" which is not well defined for single wall CNTs but it does not enter the continuum analysis, as shown in the next section.

3.3. The limit of graphene

Goze et al. (1999) used tight-binding method to investigate the effect of nanotube radius R on the Young's modulus of CNTs, and showed that, for $R > 0.4$ nm, the Young's modulus is essentially independent of the CNT radius. Jiang et al. (2003) also showed that the CNT radius has essentially no effect on the Young's modulus nor on the load-deflation curve of CNTs under tension or torsion. In the limit of large CNT radius, a CNT becomes a graphene, i.e., a planar sheet of carbon atoms. The summation over three atomic bonds in Eq. (15) then becomes the summation over

three bond orientations within the graphene plane, ϕ_0 and $\phi_0 \pm 120°$, i.e.,

$$W(\boldsymbol{E}, \boldsymbol{\xi}) = \frac{1}{2\Omega_\varepsilon} \sum_{\phi_0, \phi_0 \pm 120°} V(r_{ij}, r_{ik}, \theta_{ijk}, k \neq i, j), \tag{17}$$

where ϕ_0 is the angle between the bond and the tube axis. In other words, (17) is the limit of Eq. (15) without accounting for the effect of CNT radius.

3.4. The shift vector $\boldsymbol{\zeta}$

The shift vector $\boldsymbol{\zeta}$ introduced in Section 3.1 (Fig. 3) relaxes the atom positions to ensure the equilibrium of atoms. For a given Lagrangian strain $\boldsymbol{E}$, the shift vector $\boldsymbol{\zeta}$ or its equivalence, the internal degree of freedom $\boldsymbol{\xi}$, is determined by minimizing the strain energy density W with respect to $\boldsymbol{\xi}$ (Weiner, 1983; Tadmor et al., 1999; Arroyo and Belytschko, 2002; Zhang et al., 2002b), i.e.,

$$\frac{\partial W}{\partial \boldsymbol{\xi}} = 0. \tag{18}$$

Eq. (18) is a nonlinear and implicit equation that is solved numerically to determine $\boldsymbol{\xi}$ in terms of $\boldsymbol{E}$, i.e.,

$$\boldsymbol{\xi} = \boldsymbol{\xi}(\boldsymbol{E}). \tag{19}$$

The strain energy density in Eqs. (15) or (17) can then be written as $W = W[\boldsymbol{E}, \boldsymbol{\xi}(\boldsymbol{E})]$. It is straightforward to verify that $\boldsymbol{\xi} = \boldsymbol{0}$ if $\boldsymbol{E} = \boldsymbol{0}$ (i.e., no deformation).

3.5. Stress and incremental modulus

The second Piola–Kirchhoff stress $\boldsymbol{T}$ is obtained from the total derivative D of strain energy density W with respect to the Lagrangian strain $\boldsymbol{E}$,

$$\boldsymbol{T} = \frac{DW}{D\boldsymbol{E}} = \frac{\partial W}{\partial \boldsymbol{E}} + \frac{\partial W}{\partial \boldsymbol{\xi}} \cdot \frac{d\boldsymbol{\xi}}{d\boldsymbol{E}} = \frac{\partial W}{\partial \boldsymbol{E}}, \tag{20}$$

where $\partial W/\partial \boldsymbol{\xi} = 0$ in Eq. (18) has been used. Eq. (20) gives the second Piola–Kirchhoff stress $\boldsymbol{T}$ in terms of the Lagrangian strain $\boldsymbol{E}$, therefore provides the constitutive relation of single wall CNTs based on the interatomic potential V.

The stress increment $\dot{\boldsymbol{T}}$ is related to the strain increment $\dot{\boldsymbol{E}}$ via the incremental modulus tensor $\boldsymbol{C}$,

$$\dot{\boldsymbol{T}} = \boldsymbol{C} : \dot{\boldsymbol{E}}, \tag{21}$$

where $\boldsymbol{C}$ is the total derivative of $\boldsymbol{T}$ with respect to $\boldsymbol{E}$, and from Eq. (20)

$$\boldsymbol{C} = \frac{D\boldsymbol{T}}{D\boldsymbol{E}} = \frac{D}{D\boldsymbol{E}} \left(\frac{\partial W}{\partial \boldsymbol{E}} \right) = \frac{\partial^2 W}{\partial \boldsymbol{E} \partial \boldsymbol{E}} - \frac{\partial^2 W}{\partial \boldsymbol{E} \partial \boldsymbol{\xi}} \cdot \left(\frac{\partial^2 W}{\partial \boldsymbol{\xi} \partial \boldsymbol{\xi}} \right)^{-1} \cdot \frac{\partial^2 W}{\partial \boldsymbol{\xi} \partial \boldsymbol{E}}, \tag{22}$$

which possesses the symmetry $C_{ijkl} = C_{jikl} = C_{ijlk} = C_{klij}$, where we have use

$$\frac{\mathrm{d}\boldsymbol{\xi}}{\mathrm{d}\boldsymbol{E}} = -\left(\frac{\partial^2 W}{\partial\boldsymbol{\xi}\partial\boldsymbol{\xi}}\right)^{-1} \cdot \left(\frac{\partial^2 W}{\partial\boldsymbol{\xi}\partial\boldsymbol{E}}\right)$$

obtained from the derivative of $\partial W/\partial\boldsymbol{\xi} = 0$ in Eq. (18).

3.6. Equilibrium equation

The equilibrium equation is

$$(\boldsymbol{F} \cdot \boldsymbol{T}) \cdot \boldsymbol{\nabla} = 0, \tag{23}$$

where $\boldsymbol{\nabla}$ is the gradient in the reference (undeformed) configuration. In the cylindrical coordinates (R, θ, Z) for the CNT, $\boldsymbol{\nabla} = \boldsymbol{e}_\mathrm{R}(\partial/\partial R) + (\boldsymbol{e}_\theta/R)(\partial/\partial\theta) + \boldsymbol{e}_Z(\partial/\partial Z)$, the equilibrium equation (23) takes the form

$$\frac{\partial}{\partial R}(\boldsymbol{F} \cdot \boldsymbol{T})_{RR} + \frac{(\boldsymbol{F} \cdot \boldsymbol{T})_{RR} - (\boldsymbol{F} \cdot \boldsymbol{T})_{\theta\theta}}{R} + \frac{1}{R}\frac{\partial}{\partial\theta}(\boldsymbol{F} \cdot \boldsymbol{T})_{R\theta} + \frac{\partial}{\partial Z}(\boldsymbol{F} \cdot \boldsymbol{T})_{RZ} = 0, \tag{24a}$$

$$\frac{\partial}{\partial R}(\boldsymbol{F} \cdot \boldsymbol{T})_{\theta R} + \frac{(\boldsymbol{F} \cdot \boldsymbol{T})_{R\theta} + (\boldsymbol{F} \cdot \boldsymbol{T})_{\theta R}}{R} + \frac{1}{R}\frac{\partial}{\partial\theta}(\boldsymbol{F} \cdot \boldsymbol{T})_{\theta\theta} + \frac{\partial}{\partial Z}(\boldsymbol{F} \cdot \boldsymbol{T})_{\theta Z} = 0, \tag{24b}$$

$$\frac{\partial}{\partial R}(\boldsymbol{F} \cdot \boldsymbol{T})_{ZR} + \frac{(\boldsymbol{F} \cdot \boldsymbol{T})_{ZR}}{R} + \frac{1}{R}\frac{\partial}{\partial\theta}(\boldsymbol{F} \cdot \boldsymbol{T})_{Z\theta} + \frac{\partial}{\partial Z}(\boldsymbol{F} \cdot \boldsymbol{T})_{ZZ} = 0. \tag{24c}$$

The traction-free boundary condition can be written as

$$(\boldsymbol{F} \cdot \boldsymbol{T}) \cdot \boldsymbol{N} = 0, \tag{25}$$

where $\boldsymbol{N}$ is the unit normal to the surface in the reference configuration. It should be pointed out that Eq. (25) has not accounted for the surface stress effect on the boundary conditions. If such an effect is accounted for, we will need to use the continuum formulation including the surface stress, such as Gurtin and Murdoch (1975). On the inner and outer surfaces of the CNT, the traction-free condition becomes

$$\boldsymbol{F} \cdot \boldsymbol{T} \cdot \boldsymbol{e}_\mathrm{R} = 0, \tag{26}$$

where $\boldsymbol{e}_\mathrm{R}$ is the unit vector in the radial direction prior to deformation. Since the single wall CNT is very thin (a single layer of atoms), $\boldsymbol{F} \cdot \boldsymbol{T} \cdot \boldsymbol{e}_\mathrm{R}$ should vanish in the entire CNT, which leads to $\boldsymbol{T} \cdot \boldsymbol{e}_\mathrm{R} = 0$ in the CNT. Therefore, the three-dimensional equilibrium equation (24) becomes

$$\frac{1}{R}\frac{\partial}{\partial\theta}(F_{R\alpha}T_{\alpha\theta}) - \frac{1}{R}F_{\theta\alpha}T_{\alpha\theta} + \frac{\partial}{\partial Z}(F_{R\alpha}T_{\alpha Z}) = 0, \tag{27a}$$

$$\frac{1}{R}F_{R\alpha}T_{\alpha\theta} + \frac{1}{R}\frac{\partial}{\partial\theta}(F_{\theta\alpha}T_{\alpha\theta}) + \frac{\partial}{\partial Z}(F_{\theta\alpha}T_{\alpha Z}) = 0, \tag{27b}$$

$$\frac{1}{R}\frac{\partial}{\partial\theta}(F_{Z\alpha}T_{\alpha\theta}) + \frac{\partial}{\partial Z}(F_{Z\alpha}T_{\alpha Z}) = 0, \tag{27c}$$

where R is the nanotube radius; and the summation for α is over θ and Z. Eq. (27) gives three partial differential equations (with respect to θ and Z) for U_R, U_θ, and U_Z, and unlike Eq. (24), they do not involve $\partial/\partial R$.

4. Fracture nucleation in single-wall CNTs

Similar to the large scattering in the Young's modulus shown in Figs. 1 and 2, the limited studies on fracture of CNTs also displayed large discrepancies in the fracture strain. For example, the atomistic studies of a single wall CNT under tension based on Brenner's (1990) empirical interatomic potential suggested the fracture strain between 25% and 55% (Yakobson et al., 1997), while Yu et al.'s (2000) experimental studies reported the fracture strain of multiwall CNTs between 2% and 13%. The recent atomistic studies of Belytschko et al. (2002) based on a different empirical interatomic potential (the modified Morse potential) predicted fracture strain from 10% to 16%. It is important to note that many factors may contribute to these discrepancies, such as single wall CNTs under simple tension in atomic studies (Yakobson et al., 1997) versus multi-wall CNTs subject to tension with possible bending in experiments (Yu et al., 2000). The different empirical interatomic potentials, such as Brenner's (1990) potential used by Yakobson et al. (1997) versus modified Morse potential used by Belytschko et al. (2002), may also lead to significantly different fracture strains.

The purpose of this paper is not to evaluate the above work on fracture of CNTs. Instead, it is to investigate whether the proposed atomistic-based continuum theory can be used to study fracture nucleation in CNTs, and whether its results agree with the atomistic studies based on the same interatomic potential without any parameter fitting.

Yakobson et al. (1997) studied a single-wall CNT under tension using MD simulations with Brenner's (1990) empirical interatomic potential for carbon. They found that there exists a breaking strain ε_b prior to which the CNT undergoes uniform deformation. Once the breaking strain is reached, one or few atomic bonds break and this atomic disorder rapidly propagates in the circumferential direction to form a necked band which eventually leads to fracture of the CNT. The breaking strain has a large variation from 25% to 55%. Zhang et al. (2002a) conducted an approximate analysis of fracture nucleation in CNTs, and several critical assumptions were made, including (i) neglecting the multi-body coupling effect by taking $B_{ij} = 1$ in the interatomic potential (1); (ii) approximating the three atomic bonds at each atom by uniformly distributed bonds over all orientations within the tube surface and therefore not accounting for the effect of the shift vector. These assumptions, in fact, do not strictly hold for single wall CNTs.

We study the breaking strain of CNTs via the atomistic-based continuum theory in the previous section established from Brenner's (1990) empirical interatomic potential. Instead of modelling the breaking of individual atomic bonds as in Yakobson et al.'s (1997) MD simulations, the continuum analysis focuses on the overall, "macroscopic" characteristics associated with the breaking strain. Since the CNT undergoes uniform

deformation prior to the first bond breaking in Yakobson et al.'s (1997) MD simulations, and nonuniform deformation only steps in after the bond breaking, fracture nucleation in CNTs under tension is modeled as a bifurcation in the present atomistic-based continuum theory.

4.1. Armchair and zigzag CNTs

4.1.1. Pre-bifurcation: uniform deformation

The deformation in armchair and zigzag CNTs under tension is uniform and axisymmetric prior to bifurcation, and is characterized by the non-vanishing components $F_{\theta\theta}$ and F_{ZZ} of the deformation gradient. The non-zero components of the Lagrangian strain are $E_{\theta\theta} = \frac{1}{2}(F_{\theta\theta}^2 - 1)$ and $E_{ZZ} = \frac{1}{2}(F_{ZZ}^2 - 1)$. The internal degree of freedom $\xi = \xi(E_{\theta\theta}, E_{ZZ})$ is determined from $\partial W / \partial \xi = 0$ in Eq. (18). The second Piola-Kirchhoff stress T is then obtained in terms of E_{ZZ} and $E_{\theta\theta}$ from Eq. (20) as

$$0 = T_{\theta\theta} = \frac{\partial W}{\partial E_{\theta\theta}}, \tag{28}$$

$$T_{ZZ} = \frac{\partial W}{\partial E_{ZZ}}, \tag{29}$$

where Eq. (28) results from the requirement that $T_{\theta\theta}$ vanishes in uniaxial tension and it is an implicit equation to determine $E_{\theta\theta}$ in terms of E_{ZZ}, i.e., $E_{\theta\theta} = E_{\theta\theta}(E_{ZZ})$. The non-zero components of the incremental modulus $C_{\theta\theta\theta\theta}$, C_{ZZZZ}, $C_{\theta\theta ZZ} = C_{ZZ\theta\theta}$ and $C_{\theta Z\theta Z}$ are obtained from Eq. (22).

4.1.2. Onset of bifurcation: nonuniform increment of deformation

Let U denote the displacement, which is related to the deformation gradient F by $F = I + U\nabla$. At the onset of bifurcation, the increment of deformation is not uniform anymore. The non-uniform increment of deformation gradient $\dot{F}$ is given in terms of the displacement increment $\dot{U}$ by

$$\dot{F}_{R\theta} = \frac{1}{R}\frac{\partial \dot{U}_R}{\partial \theta} - \frac{\dot{U}_\theta}{R}, \quad \dot{F}_{\theta\theta} = \frac{\dot{U}_R}{R} + \frac{1}{R}\frac{\partial \dot{U}_\theta}{\partial \theta}, \quad \dot{F}_{Z\theta} = \frac{1}{R}\frac{\partial \dot{U}_Z}{\partial \theta},$$

$$\dot{F}_{RZ} = \frac{\partial \dot{U}_R}{\partial Z}, \quad \dot{F}_{\theta Z} = \frac{\partial \dot{U}_\theta}{\partial Z}, \quad \dot{F}_{ZZ} = \frac{\partial \dot{U}_Z}{\partial Z}, \tag{30}$$

where only the components within the tube surface are given. The corresponding non-zero components of the Lagrangian strain increment $\dot{E}$ are

$$\dot{E}_{\theta\theta} = F_{\theta\theta}\dot{F}_{\theta\theta}, \tag{31a}$$

$$\dot{E}_{ZZ} = F_{ZZ}\dot{F}_{ZZ}, \tag{31b}$$

$$\dot{E}_{\theta Z} = \dot{E}_{Z\theta} = \frac{1}{2}(F_{\theta\theta}\dot{F}_{\theta Z} + F_{ZZ}\dot{F}_{Z\theta}), \tag{31c}$$

where $F_{\theta Z} = 0$ at the onset of bifurcation has been used.

The non-vanishing components of the stress increment are obtained from Eq. (21) as

$$\dot{T}_{\theta\theta} = C_{\theta\theta\theta\theta}\dot{E}_{\theta\theta} + C_{\theta\theta ZZ}\dot{E}_{ZZ}, \tag{32a}$$

$$\dot{T}_{ZZ} = C_{ZZ\theta\theta}\dot{E}_{\theta\theta} + C_{ZZZZ}\dot{E}_{ZZ}, \tag{32b}$$

$$\dot{T}_{\theta Z} = \dot{T}_{Z\theta} = 2C_{\theta Z\theta Z}\dot{E}_{\theta Z}. \tag{32c}$$

The substitution of Eqs. (30), (31) and (32) into the incremental form of the equilibrium equation (27) gives

$$\left(T_{ZZ}\frac{\partial^2}{\partial Z^2} - \frac{1}{R^2}C_{\theta\theta\theta\theta}F_{\theta\theta}^2\right)\dot{U}_R - \frac{1}{R^2}C_{\theta\theta\theta\theta}F_{\theta\theta}^2\frac{\partial\dot{U}_\theta}{\partial\theta}$$
$$-\frac{1}{R}C_{\theta\theta ZZ}F_{\theta\theta}F_{ZZ}\frac{\partial\dot{U}_Z}{\partial Z} = 0, \tag{33a}$$

$$\frac{1}{R^2}C_{\theta\theta\theta\theta}F_{\theta\theta}^2\frac{\partial\dot{U}_R}{\partial\theta} + \left[\frac{1}{R^2}C_{\theta\theta\theta\theta}F_{\theta\theta}^2\frac{\partial^2}{\partial\theta^2} + (T_{ZZ} + C_{\theta Z\theta Z}F_{\theta\theta}^2)\frac{\partial^2}{\partial Z^2}\right]\dot{U}_\theta$$
$$+\frac{1}{R}(C_{\theta\theta ZZ} + C_{\theta Z\theta Z})F_{\theta\theta}F_{ZZ}\frac{\partial^2\dot{U}_Z}{\partial\theta\partial Z} = 0, \tag{33b}$$

$$\frac{1}{R}C_{\theta\theta ZZ}F_{\theta\theta}F_{ZZ}\frac{\partial\dot{U}_R}{\partial Z} + \frac{1}{R}(C_{\theta\theta ZZ} + C_{\theta Z\theta Z})F_{\theta\theta}F_{ZZ}\frac{\partial^2\dot{U}_\theta}{\partial\theta\partial Z}$$
$$+\left[\frac{1}{R^2}C_{\theta Z\theta Z}F_{ZZ}^2\frac{\partial^2}{\partial\theta^2} + (T_{ZZ} + C_{ZZZZ}F_{ZZ}^2)\frac{\partial^2}{\partial Z^2}\right]\dot{U}_Z = 0. \tag{33c}$$

The CNT is subjected to the axial displacement and vanishing shear stress tractions at the ends. Therefore, at the onset of bifurcation, the increments of the axial displacement and shear stress tractions vanish at both ends. The increment of stress tractions at the ends of the CNT can be obtained from Eq. (25) as $\dot{F} \cdot T \cdot e_Z + F \cdot \dot{T} \cdot e_Z$ such that the vanishing of increments of shear stress tractions gives $\dot{F}_{RZ}T_{ZZ} = 0$ and $\dot{F}_{\theta Z}T_{ZZ} + F_{\theta\theta}\dot{T}_{\theta Z} = 0$ in the $R-$ and $\theta-$ directions, respectively. In conjunction with Eq. (30), the incremental boundary conditions at the two ends of the CNT can be written as

$$\dot{U}_Z = \frac{\partial\dot{U}_R}{\partial Z} = \frac{\partial\dot{U}_\theta}{\partial Z} = 0 \quad \text{at } Z = 0 \text{ and } Z = L, \tag{34}$$

where L is the length of the CNT.

The homogeneous governing equations (33) and boundary conditions (34) constitute an eigenvalue problem for the displacement increment $\dot{U}$. The eigenvalue is the axial strain E_{ZZ} (or equivalently, F_{ZZ}). In other words, Eqs. (33) and (34) have only the trivial solution $\dot{U} = 0$ until the axial strain E_{ZZ} reaches a critical value $(E_{ZZ})_{\text{critical}}$ for bifurcation.

4.1.3. Axisymmetric bifurcation

We first study the axisymmetric bifurcation, $\dot{U}_R = \dot{U}_R(Z)$, $\dot{U}_\theta = 0$, and $\dot{U}_Z = \dot{U}_Z(Z)$. The governing equation (33) becomes

$$\left(T_{ZZ} \frac{d^2}{dZ^2} - \frac{1}{R^2} C_{\theta\theta\theta\theta} F_{\theta\theta}^2 \right) \dot{U}_R - \frac{1}{R} C_{\theta\theta ZZ} F_{\theta\theta} F_{ZZ} \frac{d\dot{U}_Z}{dZ} = 0, \tag{35a}$$

$$\frac{1}{R} C_{\theta\theta ZZ} F_{\theta\theta} F_{ZZ} \frac{d\dot{U}_R}{dZ} + (T_{ZZ} + C_{ZZZZ} F_{ZZ}^2) \frac{d^2\dot{U}_Z}{dZ^2} = 0. \tag{35b}$$

Its solution, satisfying the homogeneous boundary condition (34), takes the form

$$[\dot{U}_R, \dot{U}_Z] = \left[\dot{U}_{Rm}^{(0)} \cos \frac{m\pi Z}{L}, \dot{U}_{Zm}^{(0)} \sin \frac{m\pi Z}{L} \right], \tag{36}$$

where $m = 1, 2, 3, \ldots$ is the eigen mode number, $[\dot{U}_{Rm}^{(0)}, \dot{U}_{Zm}^{(0)}]$ is the corresponding eigenvector, and the superscript (0) denotes the axisymmetric bifurcation. The substitution of Eq. (36) into Eq. (35) yields two homogeneous, linear algebraic equations for $\dot{U}_{Rm}^{(0)}$ and $\dot{U}_{Zm}^{(0)}$. In order to have a non-trivial solution, the determinant of the 2×2 coefficient matrix for the linear algebraic equations must vanish. This gives the critical condition for bifurcation as

$$f^{(0)} \equiv C_{\theta\theta\theta\theta} \left(C_{ZZZZ} + \frac{T_{ZZ}}{F_{ZZ}^2} \right) - C_{\theta\theta ZZ}^2 + \frac{T_{ZZ}}{F_{\theta\theta}^2} \left(C_{ZZZZ} + \frac{T_{ZZ}}{F_{ZZ}^2} \right) \left(\frac{m\pi R}{L} \right)^2 = 0. \tag{37}$$

The above equation, in conjunction with $T_{\theta\theta} = 0$ in Eq. (28), provides two equations to determine $E_{\theta\theta}$ and E_{ZZ} (or equivalently $F_{\theta\theta}$ and F_{ZZ}) at the onset of bifurcation. The corresponding axial strain at bifurcation is denoted by $(E_{ZZ})_{\text{critical}}$.

It is pointed out that the bifurcation condition (37) is independent of the CNT wall thickness t_0 introduced in Eq. (16). This is because both Eqs. (37) and (28) are homogeneous with respect to the stress $\boldsymbol{T}$ and incremental modulus $\boldsymbol{C}$, and $\boldsymbol{T}$ and $\boldsymbol{C}$ are both proportional to t_0^{-1}, as observed from Eqs. (20) and (22).

4.1.4. Non-axisymmetric bifurcation

For non-axisymmetric bifurcation, the displacement increment takes the form

$$[\dot{U}_R, \dot{U}_\theta, \dot{U}_Z] = [\dot{U}_R^{(n)}(Z) \cos n\theta, \dot{U}_\theta^{(n)}(Z) \sin n\theta, \dot{U}_Z^{(n)}(Z) \cos n\theta], \tag{38}$$

where $n = 1, 2, 3, \ldots$ is the wave number in the circumferential direction, $\dot{U}_R^{(n)}$, $\dot{U}_\theta^{(n)}$, and $\dot{U}_Z^{(n)}$ are functions of Z to be determined. For $n = 0$, Eq. (38) degenerates to Eq. (36) for axisymmetric bifurcation. The general solution of $\dot{U}_R^{(n)}$, $\dot{U}_\theta^{(n)}$ and $\dot{U}_Z^{(n)}$, satisfying the homogeneous boundary condition (34), takes the form

$$[\dot{U}_R^{(n)}, \dot{U}_\theta^{(n)}, \dot{U}_Z^{(n)}] = \left[\dot{U}_{Rm}^{(n)} \cos \frac{m\pi Z}{L}, \dot{U}_{\theta m}^{(n)} \cos \frac{m\pi Z}{L}, \dot{U}_{Zm}^{(n)} \sin \frac{m\pi Z}{L} \right], \tag{39}$$
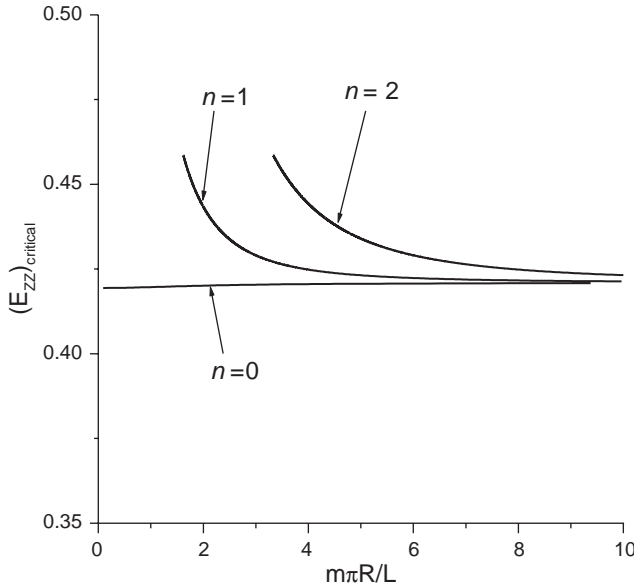
Fig. 5. Bifurcation strain for armchair CNTs.

where $m = 1, 2, 3, \ldots$ is the eigen mode number in the axial direction, and $[\dot{U}_{Rm}^{(n)}, \dot{U}_{\theta m}^{(n)}, \dot{U}_{Zm}^{(n)}]$ is the corresponding eigenvector. The substitution of Eqs. (38) and (39) into the incremental equilibrium equation (33) yields three homogeneous, linear algebraic equations for $\dot{U}_{Rm}^{(n)}$, $\dot{U}_{\theta m}^{(n)}$ and $\dot{U}_{Zm}^{(n)}$. In order to have a non-trivial solution, the determinant of the corresponding 3×3 coefficient matrix must vanish. This gives the bifurcation condition as

$$f^{(n)} \equiv f^{(0)} + \frac{n^2 T_{ZZ}}{T_{ZZ} + C_{\theta Z \theta Z} F_{\theta \theta}^2} \left[C_{\theta \theta \theta \theta} \left(C_{ZZZZ} + \frac{T_{ZZ}}{F_{ZZ}^2} \right) - (C_{\theta \theta ZZ} + C_{\theta Z \theta Z})^2 \right.$$

$$\left. + C_{\theta Z \theta Z} \left(C_{\theta Z \theta Z} + \frac{T_{ZZ}}{F_{\theta \theta}^2} \right) + (n^2 + 1) C_{\theta \theta \theta \theta} C_{\theta Z \theta Z} \left(\frac{L}{m \pi R} \right)^2 \right] = 0, \qquad (40)$$

where $f^{(0)}$ is the function in Eq. (37) defined for axisymmetric bifurcation ($n = 0$). The critical bifurcation strains $(E_{\theta \theta})_{\text{critical}}$ and $(E_{ZZ})_{\text{critical}}$ at the onset of bifurcation are determined from Eqs. (28) and (40).

4.1.5. Bifurcation strain

Fig. 5 shows the bifurcation strain $(E_{ZZ})_{\text{critical}}$ versus $m \pi R / L$ for armchair CNTs, where m ($=1, 2, 3, \ldots$) is the eigen mode number in the axial direction, and R and L are the radius and length of the CNT, respectively. Both the axisymmetric bifurcation strain ($n = 0$) and non-axisymmetric bifurcation strain ($n = 1, 2, 3, \ldots$) from Eq. (40) are presented. The axisymmetric bifurcation ($n = 0$) gives the lowest bifurcation strain
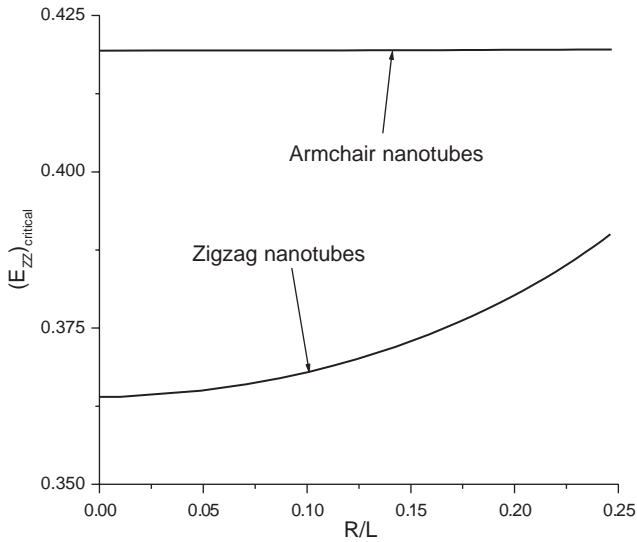
Fig. 6. Bifurcation strain for armchair and zigzag CNTs.

such that the armchair CNTs always bifurcate in the axisymmetric form. For $n = 0$, the bifurcation strain increases very slowly with $m\pi R/L$ and is essentially a constant, 0.42. Fig. 5 also indicates that the bifurcation takes place with the first mode ($m = 1$) in the axial direction and the axisymmetric mode ($n = 0$) in the circumferential direction. This is because the curve for $n = 0$ in Fig. 5 increases monotonically (though slowly) with $m\pi R/L$ such that, at each fixed R/L, the first eigen mode $m = 1$ in the axial direction gives the smallest bifurcation strain. Since the CNT length is at least twice its diameter, $L \geqslant 4R$, the bifurcation strain (corresponding to $n = 0$ and $m = 1$) is replotted in Fig. 6 for R/L less than 0.25.

Fig. 6 also shows the bifurcation strain $(E_{ZZ})_{\text{critical}}$ for zigzag CNTs, where R and L are the radius and length of the CNT, respectively. The bifurcation also takes place with the first eigen mode ($m = 1$) in the axial direction and the axisymmetric mode ($n = 0$) in the circumferential direction. The bifurcation strain for zigzag CNTs displays a stronger dependence on the tube aspect ratio than the armchair CNTs, and it increases with R/L. For a 1 nm diameter ($R = 0.5$ nm) and 5 nm long nanotube, the bifurcation strain predicted by the present atomistic-based continuum theory is around 0.37. This is within the range of the breaking strains reported by Yakobson et al.'s (1997) MD simulations for the same tube aspect ratio.

For a fixed CNT aspect ratio R/L, we have calculated the bifurcation strain with two different constitutive models of CNTs, Eq. (15) which accounts for the effect of finite CNT radius and Eq. (17) which neglects such effect in the constitutive relation. The numerical results show that these two models predict identical bifurcation strains for CNTs with radius > 0.35 nm. Therefore, the CNT radius (> 0.35 nm) has essentially no effect on the bifurcation strain.

4.2. Chiral CNTs

4.2.1. Pre-bifurcation: uniform deformation

The deformation prior to bifurcation is uniform. The non-zero components of the Lagrangian strain are $E_{\theta\theta}$ and E_{ZZ}, but the shear stress $T_{\theta Z}$ does not vanish anymore because chiral CNTs give anisotropic material behavior. The stress is obtained from Eq. (20), and the vanishing of stress $T_{\theta\theta} = 0$ gives $E_{\theta\theta}$ in terms of E_{ZZ}, i.e., $E_{\theta\theta} = E_{\theta\theta}(E_{ZZ})$. The non-zero components of the incremental modulus obtained from Eq. (22) are $C_{\theta\theta\theta\theta}$, C_{ZZZZ}, $C_{\theta\theta ZZ} = C_{ZZ\theta\theta}$, $C_{\theta Z\theta Z}$, $C_{\theta\theta\theta Z} = C_{\theta Z\theta\theta}$ and $C_{ZZZ\theta} = C_{\theta ZZZ}$.

4.2.2. Onset of bifurcation: nonuniform increment of deformation

The increment of deformation gradient and Lagrangian strain are still given by Eqs. (30) and (31), respectively. The stress increment in Eq. (32) becomes

$$\dot{T}_{\theta\theta} = C_{\theta\theta\theta\theta}\dot{E}_{\theta\theta} + C_{\theta\theta ZZ}\dot{E}_{ZZ} + 2C_{\theta\theta\theta Z}\dot{E}_{\theta Z}, \tag{41a}$$

$$\dot{T}_{ZZ} = C_{ZZ\theta\theta}\dot{E}_{\theta\theta} + C_{ZZZZ}\dot{E}_{ZZ} + 2C_{ZZZ\theta}\dot{E}_{\theta Z}, \tag{41b}$$

$$\dot{T}_{\theta Z} = \dot{T}_{Z\theta} = C_{Z\theta\theta\theta}\dot{E}_{\theta\theta} + C_{\theta ZZZ}\dot{E}_{ZZ} + 2C_{\theta Z\theta Z}\dot{E}_{\theta Z}. \tag{41c}$$

The equilibrium equation (33) gives

$$\left(-\frac{1}{R^2} C_{\theta\theta\theta\theta}F_{\theta\theta}^2 + \frac{2}{R} T_{\theta z} \frac{\partial^2}{\partial\theta\partial Z} + T_{ZZ} \frac{\partial^2}{\partial Z^2}\right)\dot{U}_Z$$

$$+ \frac{1}{R}\left[-\frac{1}{R} C_{\theta\theta\theta\theta}F_{\theta\theta}^2 \frac{\partial}{\partial\theta} - (C_{\theta\theta\theta Z}F_{\theta\theta}^2 + 2T_{\theta Z}) \frac{\partial}{\partial Z}\right]\dot{U}_\theta$$

$$+ \frac{1}{R} F_{\theta\theta}F_{ZZ}\left(-\frac{1}{R} C_{\theta\theta\theta Z} \frac{\partial}{\partial\theta} - C_{\theta\theta ZZ} \frac{\partial}{\partial Z}\right)\dot{U}_Z = 0, \tag{42a}$$

$$\frac{1}{R}\left[\frac{1}{R} C_{\theta\theta\theta\theta}F_{\theta\theta}^2 \frac{\partial}{\partial\theta} + (C_{\theta\theta\theta Z}F_{\theta\theta}^2 + 2T_{\theta Z}) \frac{\partial}{\partial Z}\right]\dot{U}_R$$

$$+ \left[\frac{1}{R^2} C_{\theta\theta\theta\theta}F_{\theta\theta}^2 \frac{\partial^2}{\partial\theta^2} + \frac{2}{R}(C_{\theta\theta\theta Z}F_{\theta\theta}^2 + T_{\theta Z}) \frac{\partial^2}{\partial\theta\partial Z} + (C_{\theta Z\theta Z}F_{\theta\theta}^2 + T_{ZZ}) \frac{\partial^2}{\partial Z^2}\right]\dot{U}_\theta$$

$$+ F_{\theta\theta}F_{ZZ}\left[\frac{1}{R^2} C_{\theta\theta\theta Z} \frac{\partial^2}{\partial\theta^2} + \frac{1}{R}(C_{\theta\theta ZZ} + C_{\theta Z\theta Z}) \frac{\partial^2}{\partial\theta\partial Z} + C_{\theta ZZZ} \frac{\partial^2}{\partial Z^2}\right]\dot{U}_Z = 0, \tag{42b}$$

$$\frac{1}{R} F_{\theta\theta}F_{ZZ}\left(\frac{1}{R^2} C_{\theta\theta\theta Z} \frac{\partial}{\partial\theta} + \frac{1}{R} C_{\theta\theta ZZ} \frac{\partial}{\partial Z}\right)\dot{U}_R$$

$$+ F_{\theta\theta}F_{ZZ}\left[\frac{1}{R^2} C_{\theta\theta\theta Z} \frac{\partial^2}{\partial\theta^2} + \frac{1}{R}(C_{\theta\theta ZZ} + C_{\theta Z\theta Z}) \frac{\partial^2}{\partial\theta\partial Z} + C_{\theta ZZZ} \frac{\partial^2}{\partial Z^2}\right]\dot{U}_\theta$$
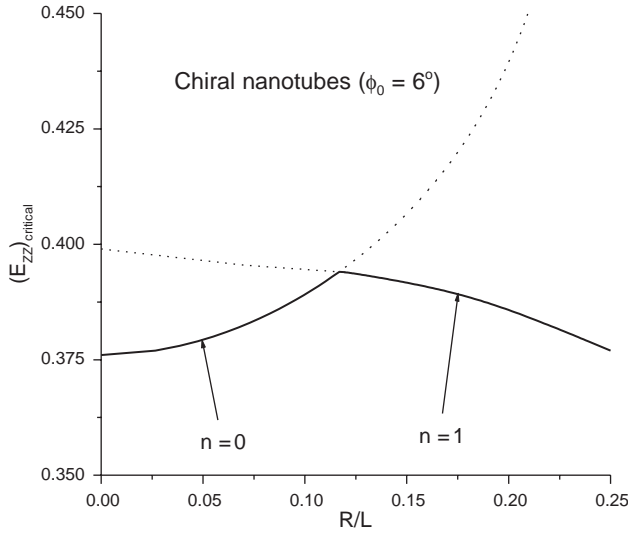
Fig. 7. Bifurcation strain for chiral CNTs.

$$+ \left[\frac{1}{R^2} C_{\theta Z\theta Z} F_{ZZ}^2 \frac{\partial^2}{\partial \theta^2} + \frac{2}{R} (C_{\theta ZZZ} F_{ZZ}^2 + T_{\theta Z}) \frac{\partial^2}{\partial \theta \partial Z} \right.$$

$$\left. + (C_{ZZZZ} F_{ZZ}^2 + T_{ZZ}) \frac{\partial^2}{\partial Z^2} \right] \dot{U}_Z = 0. \tag{42c}$$

The boundary conditions in Eq. (34) becomes

$$\dot{U}_Z = \frac{\partial \dot{U}_R}{\partial Z} + \frac{T_{\theta Z}}{T_{ZZ}} \frac{1}{R} \left(\frac{\partial \dot{U}_R}{\partial \theta} - \dot{U}_\theta \right) = \frac{\partial \dot{U}_\theta}{\partial Z} = 0$$

$$\text{at } Z = 0 \text{ and } Z = L. \tag{43}$$

The homogeneous equations (42) and boundary conditions (43) constitute an eigenvalue problem. They have a non-trivial solution only when the axial strain E_{ZZ} reaches the eigenvalue, $(E_{ZZ})_{\text{critical}}$, for bifurcation.

4.2.3. Bifurcation strain

The method to solve the above eigenvalue problem is the same as that in the previous section. The displacement increment is written as $\dot{U}_s^{(n)}(Z) \sin n\theta + \dot{U}_c^{(n)}(Z) \cos n\theta$, and (42) then gives ordinary differential equations for $\dot{U}_s^{(n)}$ and $\dot{U}_c^{(n)}$. Details of the solution method are not presented here.

Fig. 7 shows the bifurcation strain $(E_{ZZ})_{\text{critical}}$ versus the tube radius-to-length ratio, R/L, for chiral CNTs with the chiral angle $\phi_0 = 6°$, where ϕ_0 is the angle between the tube axis and a bond. For $R/L < 0.118$, the axisymmetric bifurcation ($n=0$) occurs, and the bifurcation strain increases with R/L (similar to zigzag CNTs in Fig. 6). However, for $R/L > 0.118$, the first non-axisymmetric mode ($n=1$) takes place, and the bifurcation

strain decreases with the increasing R/L. Contrary to armchair and zigzag CNTs, the first non-axisymmetric bifurcation mode can be activated in chiral CNTs, though higher modes ($n \geqslant 2$) never take place. We have studied other chiral nanotubes with the chiral angle ϕ_0 between $0°$ and $30°$, and have also observed that the non-axisymmetric bifurcation may be activated.

5. The cutoff function

The cutoff function f_c in Eq. (4) introduces a dramatic increase in the interatomic force at the cutoff distance $R^{(1)} = 0.17$ nm (Belytschko et al., 2002). This strange feature in the force is a result of the cutoff function on the interatomic potential. In order to avoid this unphysical feature, Belytschko et al. (2002) used the modified Morse potential instead, while Shenderova et al. (2000) used a larger cutoff distance in Brenner's (1990) interatomic potential. Since the cutoff function in Eq. (4) has a discontinuous second order derivative, the incremental modulus tensor $\boldsymbol{C}$ in Eq. (22) is also discontinuous at the cutoff distance 0.17 nm, and this may influence the bifurcation strain predicted by the present analysis. To exclude this artificial effect of the cutoff function f_c, we do not use the cutoff function in this paper. The results presented in Figs. 5–7 are obtained with f_c replaced by unity (one). Since the bifurcation still occurs without the cutoff function, it must be intrinsic to CNTs under tension.

The important question now is whether the bifurcation strain will change significantly if the cutoff function is used. For zigzag CNTs, we have found all three bond lengths at the bifurcation strain 0.37 [accounting for the shift vector $\boldsymbol{\zeta}$, or equivalently $\boldsymbol{\xi}$ as in Eq. (19)] to be less than the cutoff distance 0.17 nm, which means the predicted bifurcation strain will remain the same even if the cutoff function is used. However, for armchair CNTs, two bond lengths are larger than the cutoff distance 0.17 nm at the predicted bifurcation strain 0.42, which suggests that the cutoff function may influence the predicted bifurcation strain. In fact, our calculations accounting for the cutoff function show that the bifurcation strain becomes 0.50 for armchair CNTs. This value agrees well with the maximum fracture nucleation strain for armchair CNTs reported in MD simulations with the cutoff function (Yakobson et al., 1997), but is higher than 0.42 reported in Fig. 5 without the cutoff function. Therefore, even though the bifurcation is intrinsic to CNTs under tension, the bifurcation strain predicted may depend on the cutoff function.

It is noted that the bifurcation strain 0.37 reported in Fig. 6 is still higher than the fracture strain reported in Belytschko et al.'s (2002) MD simulations based on the modified Morse potential and in Dumitrica et al.'s (2003) tight binding calculations. The use of different potentials may be responsible for this difference.

6. Concluding remarks

We have proposed an atomistic-based continuum theory for CNTs based on the interatomic potential. It links the continuum constitutive model for CNTs to the interatomic

potential of carbon (Brenner, 1990). We have applied the atomistic-based continuum theory to model fracture nucleation in single-wall CNTs under tension as a bifurcation problem. The results agree reasonably well with MD simulations without any parameter fitting. The proposed approach to link continuum analysis to the interatomic potential can be applied to other nano-structured materials if the interatomic potential and the atomic structure are known.

Acknowledgements

References

Arroyo, M., Belytschko, T., 2002. An atomistic-based finite deformation membrane for single layer crystalline films. J. Mech. Phys. Solids 50, 1941–1977.

Belytschko, T., Xiao, S.P., Schatz, G.C., Ruoff, R.S., 2002. Atomistic simulations of nanotube fracture. Phys. Rev. B 65, 235430-1–235430-8.

Born, M., Huang, K., 1954. Dynamical theory of the crystal lattices. Oxford University Press, Oxford.

Brenner, D.W., 1990. Empirical potential for hydrocarbons for use in simulating the chemical vapor deposition of diamond films. Phys. Rev. B 42, 9458–9471.

Brenner, D.W., Shenderova, O.A., Harrison, J.A., Stuart, S.J., Ni, B., Sinnott, S.B., 2002. A second-generation reactive empirical bond order (rebo) potential energy expression for hydrocarbons. J. Phys.: Condens. Matter 14, 783–802.

Cornwell, C.F., Wille, L.T., 1997. Elastic properties of single-walled carbon nanotubes in compression. Solid State Commun. 101, 555–558.

Dumitrica, T., Belytschko, T., Yakobson, B.I., 2003. Bond-breaking bifurcation states in carbon nanotube fracture. J. Chem. Phys. 118, 9485–9488.

Ebbesen, T.W., Ajayan, P.M., 1992. Large-scale synthesis of carbon nanotubes. Nature 358, 220–222.

Fan, S., Chapline, M.G., Franklin, N.R., Tombler, T., Cassell, A.M., Dai, H., 1999. Self-oriented regular arrays of carbon nanotubes and their field emission properties. Science 283, 512–514.

Gao, H., Huang, Y., Abraham, F.A., 2001. Continuum and atomistic studies of intersonic crack propagation. J. Mech. Phys. Solids 49, 2113–2132.

Goze, C., Vaccarini, L., Henrard, L., Bernier, P., Hernandez, E., Rubio, A., 1999. Elastic and mechanical properties of carbon nanotubes. Synth. Met. 103, 2500–2501.

Gurtin, M.E., Murdoch, A.I., 1975. A continuum theory of elastic material surfaces. Arch. Ration. Mech. Anal. 57, 291–323.

Halicioglu, T., 1998. Stress calculations for carbon nanotubes. Thin Solid Films 312, 11–14.

Hernández, E., Goze, C., Bernier, P., Rubio, A., 1998. Elastic properties of C and BxCyNz composite nanotubes. Phys. Rev. Lett. 80, 4502–4505.

Hernández, E., Goze, C., Bernier, P., Rubio, A., 1999. Elastic properties of single-wall nanotubes. Appl. Phys. A 68, 287–292.

Iijima, S., 1991. Helical microtubules of graphite carbon. Nature 354, 56–58.

Jiang, H., Zhang, P., Liu, B., Huang, Y., Geubelle, P.H., Gao, H., Hwang, K.C., 2003. The effect of nanotube radius on the constitutive model for carbon nanotubes. Comput. Mater. Sci. 28, 429–442.

Krishnan, A., Dujardin, E., Ebbesen, T.W., Yianilos, P.N., Treacy, M.M.J., 1998. Young's modulus of single-walled nanotubes. Phys. Rev. B 58, 14013–14019.

Lier, G.V., Alsenoy, C.V., Doran, V.V., Geerlings, P., 2000. Ab intitio study of the elastic properties of single-walled carbon nanotubes and graphene. Chem. Phys. Lett. 326, 181–185.

Lourie, O., Wagner, H.D., 1998. Evaluation of young's modulus of carbon nanotubes by micro-raman soectroscopy. J. Mater. Res. 13, 2418–2422.

Lu, J.P., 1997. Elastic properties of carbon nanotubes and nanoropes. Phys. Rev. Lett. 79, 1297–1300.

Miller, R., Ortiz, M., Phillips, R., Shenoy, V., Tadmor, E.B., 1998a. Quasicontinuum models of fracture and plasticity. Eng. Fract. Mech. 61, 427–444.

Miller, R., Tadmor, E.B., Phillips, R., Ortiz, M., 1998b. Quasicontinuum simulation of fracture at the atomic scale. Modelling and Simulation in Mater. Sci. Eng. 6, 607–638.

Milstein, F., 1980. Review: theoretical elastic behaviour at large strains. J. Mater. Sci. 15, 1071–1084.

Molina, J.M., Savinsky, S.S., Khokhriakov, N.V., 1996. A tight-binding model for calculations of structures and properties of graphitic nanotubes. J. Chem. Phys. 104, 4652–4656.

Muster, J., Burghard, M., Roth, S., Duesberg, G.S., Hernández, E., Rubio, A., 1998. Scanning force microscopy characterization of individual carbon nanotubes on electrode arrays. J. Vac. Sci. Technol. B 16, 2796–2801.

Overney, G., Zhong, W., Tománek, D., 1993. Structural rigidity and low-frequency vibrational modes of long carbon tubules. Z. Phys. D: Atoms Mol. Clusters 27, 93–96.

Pan, Z.W., Xie, S.S., Lu, L., Chang, B.H., Sun, L.F., Zhou, W.Y., Wang, G., 1999. Tensile tests of ropes of very long aligned multiwall carbon nanotubes. Appl. Phys. Lett. 74, 3152–3154.

Popov, V.N., van Doren, V.E., Balkanski, M., 2000. Elastic properties of single-walled carbon nanotubes. Phys. Rev. B 61, 3078–3084.

Prylutskyy, Y.I., Durov, S.S., Ogloblya, O.V., Buzaneva, E.V., Scharff, P., 2000. Molecular dynamics simulations of mechanical, vibrational and electronic properties of carbon nanotubes. Comput. Mater. Sci. 17, 352–355.

Qian, D., Wagner, G.J., Liu, W.K., Yu, M.-F., Ruoff, R.S., 2002. Mechanics of carbon nanotubes. Appl. Mech. Rev. 55, 495–533.

Robertson, D.H., Brenner, D.W., Mintmire, J.W., 1992. Energetics of nanoscale graphitic tubules. Phys. Rev. B 45, 12592–12595.

Salvetat, J.-P., Briggs, G. AD., Bonard, J.-M., Bacsa, R.R., Kulik, A.J., 1999. Elastic and shear moduli of single-walled carbon nanotube ropes. Phys. Rev. Lett. 82, 944–947.

Sánchez-Portal, D., Artacho, E., Soler, J.M., Rubio, A., Ordejón, P., 1999. Ab Initio structural, elastic, and vibrational properties of carbon nanotubes. Phys. Rev. B 59, 12678–12688.

Shenderova, O.A., Brenner, D.W., Omeltchenko, A., Su, X., Yang, L.H., 2000. Atomistic modeling of the fracture of polycrystalline diamond. Phys. Rev. B 61, 3877–3888.

Shenoy, V.B., Miller, R., Tadmor, E.B., Phillips, R., Ortiz, M., 1998. Quasicontinuum models of interfacial structure and deformation. Phys. Rev. Lett. 80, 742–745.

Shenoy, V.B., Miller, R., Tadmor, E.B., Rodney, D., Phillips, R., Ortiz, M., 1999. An adaptive finite element approach to atomic-scale mechanics—the quasicontinuum method. J. Mech. Phys. Solids 47, 611–642.

Srivastava, D., Menon, M., Cho, K.J., 2001. Computational nanotechnology with carbon nanotubes and fullerenes. Comput. Sci. Eng. 3, 42–55.

Tadmor, E.B., Ortiz, M., Philips, R., 1996a. Quasicontinuum analysis of defects in solids. Philos. Mag. A 73, 1529–1563.

Tadmor, E.B., Philips, R., Ortiz, M., 1996b. Mixed atomistic and continuum models of deformation in solids. Langmuir 12, 4529–4534.

Tadmor, E.B., Smith, G.S., Bernstein, N., Kaxiras, E., 1999. Mixed finite element and atomistic formulation for complex crystals. Phys. Rev. B 59, 235–245.

Tersoff, J., 1988. New empirical approach for the structure and energy of covalent systems. Phys. Rev. B 37, 6991–7000.

Thess, A., Lee, R., Nikolaev, P., Dai, H.J., Petit, P., Robert, J., Xu, C.H., Lee, Y.H., Kim, S.G., Rinzler, A.G., Colbert, D.T., Scuseria, G.E., Tomanek, D., Fischer, J.E., Smalley, R.E., 1996. Crystalline ropes of metallic carbon nanotubes. Science 273, 483–487.

Tombler, T.W., Zhou, C., Alexseyev, L., Kong, J., Dai, H., Liu, L., Jayanthi, C.S., Tang, M., Wu, S.-Y., 2000. Reversible electromechanical characteristics of carbon nanotubes under local-probe manipulation. Nature 405, 769–772.

Treacy, M.M.J., Ebbesen, T.W., Gibson, J.M., 1996. Exceptionally high Young's modulus observed for individual carbon nanotubes. Nature 381, 678–680.

Vaccarini, L., Goze, C., Henrard, L., Hernández, E., Bernier, P., Rubio, A., 2000. Mechanical and electronic properties of carbon and boron-nitride nanotubes. Carbon 38, 1681–1690.

Weiner, J.H., 1983. Statistical Mechanics of Elasticity. Wiley, New York.

Wong, E.W., Sheehan, P.E., Lieber, C.M., 1997. Nanobeam mechanics: elasticity, strength, and toughness of nanorods and nanotubes. Science 277, 1971–1975.

Yakobson, B.I., Avouris, P., 2001. Mechanical properties of carbon nanotubes. In: Dresselhaus, M.S., Dresselhaus, G., Avouris, P. (Eds.), Carbon Nanotubes. Topics in Applied Physics, Vol. 80. pp. 287–329, Springer Verlag, Berlin-Heidelberg, Germany.

Yakobson, B.I., Brabec, C.J., Bernholc, J., 1996. Nanomechanics of carbon tubes: instabilities beyond linear response. Phys. Rev. Lett. 76, 2511–2514.

Yakobson, B.I., Campbell, M.P., Brabec, C.J., Bernholc, J., 1997. High strain rate fracture and C-chain unraveling in carbon nanotubes. Comput. Mater. Sci. 8, 341–348.

Yu, M.-F., Lourie, O., Dyer, M.J., Moloni, K., Kelly, T.F., Ruoff, R.S., 2000. Strength and breaking mechanism of multiwalled carbon nanotubes under tensile load. Science 287, 637–640.

Zhang, P., Huang, Y., Gao, H., Hwang, K.C., 2002a. Fracture nucleation in single-wall carbon nanotubes under tension: a continuum analysis incorporating interatomic potentials. J. Appl. Mech. 69, 454–458.

Zhang, P., Huang, Y., Geubelle, P.H., Klein, P.A., Hwang, K.C., 2002b. The elastic modulus of single-wall carbon nanotubes: a continuum analysis incorporating interatomic potentials. Int. J. Solids Struct. 39, 3893–3906.

Zhou, G., Duan, W., Gu, B., 2001. First-principles study on morphology and mechanical properties of single-walled carbon nanotube. Chem. Phys. Lett. 333, 344–349.